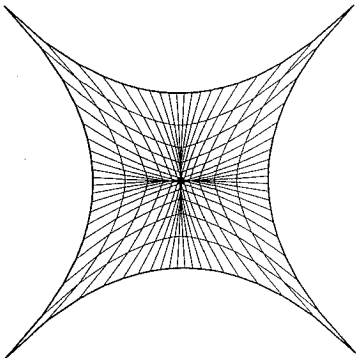

Fig. 1 Initial grid distribution generated by the linear transfinite interpolation method, 20 × 20 points, in a simple region with convex boundaries.

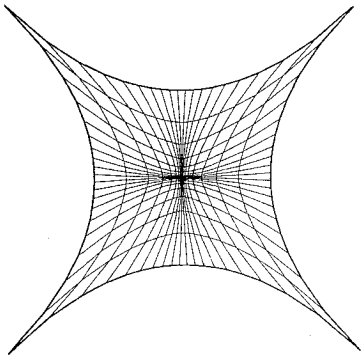

Fig. 2 Grid distribution generated by the present local grid smoothing method, ν = 10, using Fig. 1 as the initial grid system.

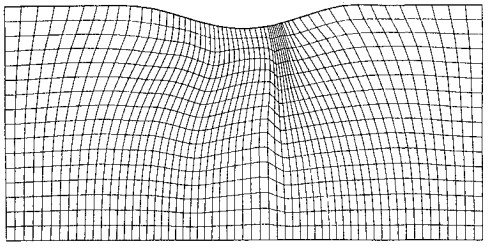

Fig. 3 Adaptive grid distribution for flow over a channel with a 10% bump, generated by the Jeng and Liou multiple one-dimensional adaptive grid scheme, 61 × 17 points, as initial data.

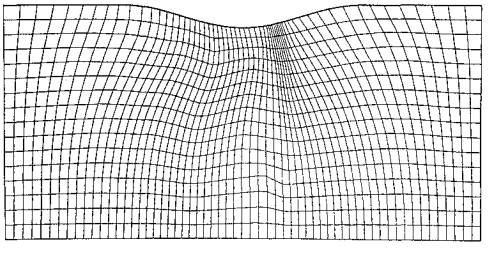

Fig. 4 Adaptive grid distribution for flow over a channel with a 10% bump, improved by the present local grid smoothing method, using Fig. 3 as the initial grid system.

fast (less than 1 s on an HP720 workstation), the grid distribution across the shock is not smooth enough, which causes the constant Mach lines to have small wiggles (not shown here) before the shock.

Instead of using the Jacobian in Eq. (3), the criterion employed here is that the intersection angle between successive grid lines should be larger than 1/10 of the maximal intersection angle of the initial grid system. The resulting grids are shown in Fig. 4, where the nonsmooothness of Fig. 3 across the shock is properly smeared. For the sake of brevity, the physical solution found by the minmod TVD scheme is not shown. Note that the Mach contours of the solution coincide with those employing the present method in the entire domain and employing the Anderson adaptive grid scheme[7,8] very well. The required CPU time for generating the adaptive grid systems of these methods are 11.8, 126.6, and 351.1 s, respectively, which demonstrates the usefulness of the present method in solving this simple problem. However, for a complex flowfield, the adaptive grid system generated by the multiple one-dimensional adaptive grid scheme may be unsatisfactory throughout the whole computing domain, and the present method can not be applied.

Conclusions

The weighted least squares method is successfully developed as a local grid smoother. The method needs an initial grid system, which is supported by fast grid schemes such as the transfinite interpolation method or the multiple one-dimensional adaptive grid scheme. Numerical evidence illustrates that the proposed method properly smoothes out the initial grids and preserves the initial grid clustering and stretching. Therefore, the applicability of these two fast schemes is greatly improved.

Acknowledgment

The work presented herein was supported by Taiwan FDID Grant 80-F008.

References

[1]Thompson, J. F., Thames, F. C., and Mastin, C. W., "Boundary-Fitted Coordinate Systems for Numerical Solution of Partial Differential Equations—A Review," *Journal of Computational Physics*, Vol. 47, No. 1, 1982, pp. 1–108.

[2]Eriksson, L. E., "Generation of Boundary-Conforming Grids Around Wing-Body Configuration Using Transfinite Interpolation," *AIAA Journal*, Vol. 20, No. 10, 1982, pp. 1313–1320.

[3]Burden, R. L., Faires, J. D., and Reynolds, A C. (eds.), *Numerical Analysis*, Prindle, Weber and Schmidt, 1978, pp. 156–163.

[4]Shyy, W., " An Adaptive Grid Method for Navier-Stokes Flow Computation," *Applied Mathematics and Computation*, Vol. 21, No. 3, 1987, pp. 201–219.

[5]Jeng, Y. N., and Liou, S. C., "Modified Multiple One-Dimensional Adaptive Grid Method," *Numerical Heat Transfer*, Pt. B, Vol. 15, No. 2, 1989, pp. 241–247.

[6]Yee, H. C., and Harten, A., "Implicit TVD Schemes for Hypersonic Conservation Laws in Curvilinear Coordinates," *AIAA Journal*, Vol. 25, No. 2, 1987, pp. 266–274.

[7]Anderson, D. A., "Equidstribution Schemes, Poisson Generators and Adaptive Grids," *Applied Mathematics and Computation*, Vol. 24, No. 3, 1987, pp. 211–227.

[8]Anderson, D. A., "Adaptive Grid Scheme Controlling Cell Area/Volume," AIAA Paper 87-0202, Jan. 1987.

Jet Mixing Control Using Excitation from Miniature Oscillating Jets

Ganesh Raman*
NYMA Inc., Brookpark, Ohio 44142
and
David Cornelius†
Stanford University, Stanford, California 94305

Introduction

THE viability and performance of an unsteady fluid-dynamic excitation system were investigated. The objective was to develop and successfully demonstrate the use of excitation devices for the

Received March 10, 1994; revision received Aug. 2, 1994; accepted for publication Sept. 6, 1994.

*Senior Research Engineer, NASA Lewis Research Center Group, Experimental Fluid Dynamics Section. Member AIAA.

†Graduate Student, Department of Aeronautics and Astronautics; NASA/OAI Summer Student Intern at NASA Lewis Research Center, Cleveland, OH 44135.

control of shear flows in practical applications. Many researchers[1,2] have used acoustic drivers for laboratory studies of jet mixing enhancement. Although convenient and easy to use, acoustic drivers are not suitable for controlling flows of practical interest due to their enormous weight, power, and maintenance requirements. In addition, as the Mach number, background noise, and turbulence levels increase, the excitation amplitude provided by acoustic drivers would prove insufficient. A practical excitation device should ideally have minimum power requirements and no moving parts, and should produce excitation that is controllable in frequency, amplitude, and phase. It appears that fluidic oscillators can satisfy these requirements.

Early work on the fluidic oscillator nozzle (better known as the flip-flop jet nozzle) was done in 1975 by Viets.[3] He showed that it is possible to produce and sustain an oscillating jet flow without any moving parts. The use of flip-flop jet nozzles as excitation devices was suggested in a review article by Rice and Zaman.[4] Previous work[5–7] focused on developing an understanding of fluidic excitation devices. In the present work we actually used such miniature fluidic devices to excite a jet flow. To our knowledge, such an experiment has not been reported before.

Davis[8] reported a study of jet decay using radial blowing from a pair of steady control jets operated in two velocity regimes. Brown and Ahuja[9] performed a novel experiment by applying hydrodynamic excitation using a vortex generator ring located in the annular stream of a coannular jet. The present work uses the hydrodynamic excitation idea of Brown and Ahuja[9] as well as the mass addition idea of Davis.[8]

Experimental Apparatus and Procedure

A schematic of the fluidic jet nozzle is shown in Fig. 1a. The nozzle and facility were described in an earlier paper.[6] Therefore, only a brief description is given here. The fluidic jet outer nozzle attachment, with exit dimensions H (7 mm) and B (19.05 mm), is affixed to the end of the inner convergent rectangular slot nozzle with exit dimensions h (2.34 mm) and b (19.05 mm). A feedback tube of length L (71 cm) and diameter d (10.7 mm) connects the control ports of width w (3.17 mm) located on the outer nozzle attachment (length, L_{ff} = 15.87 mm). Flow from the inner nozzle, issuing between the two plates of the nozzle attachment, could attach to either wall due to the Coanda effect. The equalization of pressures provided by the feedback tube causes the jet to detach from one wall and attach to the other. Thus, an oscillating jet flow is achieved. Details of the operation of such nozzles, including the effect of feedback tube length, volume, and jet velocity on the frequency of oscillation, can be found in the work by Viets[3] and Raman et al.[5,6] The primary rectangular nozzle had an equivalent diameter D_e of 4.37 cm (2.236 × 6.708 cm), an aspect ratio of 3, and was operated at an exit velocity of 48.76 m/s, which corresponds to a $Re(D_e)$ of 134,000. The fluidic jets were located approximately 1.4 D_e away from the primary jet (on either side). The centerline of each exciter jet was oriented at 30 deg to the centerline axis of the main jet (see Figs. 1b and 1c). Air supply to each of the two fluidic jets, as well as the primary jet, could be controlled independently. The velocity measured at the exit of each fluidic jet was 70 m/s. The corresponding mass flow through each fluidic jet was approximately 12% of that through the primary jet. The sinuous mode (antisymmetric in u' and symmetric in v') was forced by operating the two fluidic jets in phase (Fig. 1b). In contrast, the varicose mode (symmetric in u' and antisymmetric in v') was forced by operating the fluidic jets out of phase (Fig. 1c). Details of the fluidic jet interconnection schemes that produce in-phase or out-of-phase forcing can be found in Ref. 7.

A United sensor boundary-layer probe (Model BR-020-12-C11-120) was used for boundary-layer measurements. A hot-film probe (TSI 1210-20) was used to measure the velocity perturbation levels produced by the fluidic device, and a Kiel pressure probe (KAC-12) was used for flowfield measurements.

Discussion of Results

Figure 2 shows the velocity spectrum that was obtained using a hot-film probe placed downstream of the fluidic nozzle. The fluidic oscillator used here, due to its on-off (square wave) behavior,

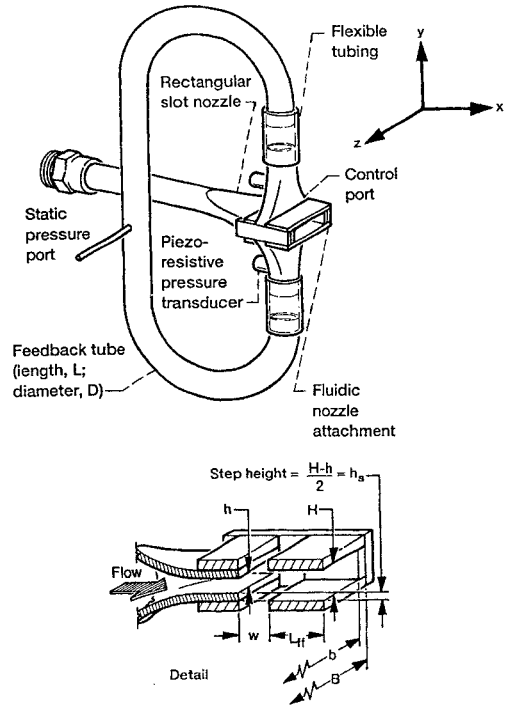

Fig. 1 Schematic of fluidic jet nozzle and excitation configurations: a) fluidic jet nozzle, b) configuration for sinous mode forcing, and c) configuration for varicose mode forcing.

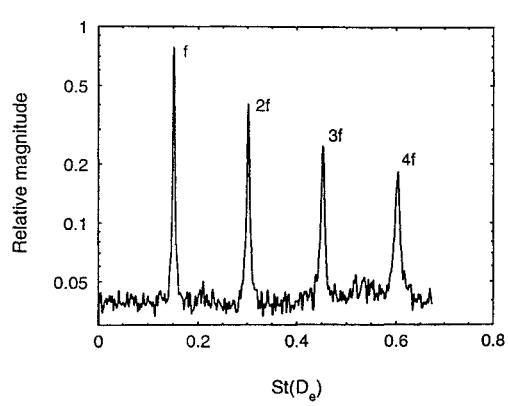

Fig. 2 Velocity spectrum of a fluidic jet measured at x/D_e = 0.6, y/D_e = 0.25, and z/D_e = 0.

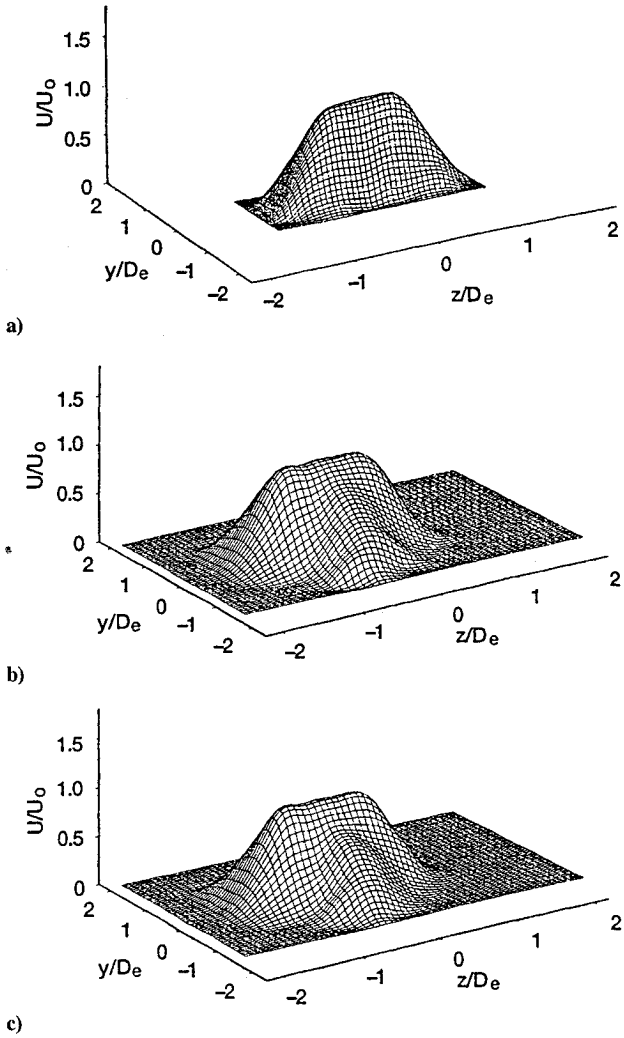

Fig. 3 Mean velocity data at x/D_e = 3: a) Unforced primary jet, b) primary jet excited in the sinous mode, and c) primary jet excited in the varicose mode.

produced excitation at 170 Hz and three higher harmonics, which covered a Strouhal number $St(D_e)$ range of 0.15–0.6. Crow and Champagne[1] defined the preferred mode for jet excitation at an $St(D_e)$ of 0.3. Note that the operating conditions and dimensions of the primary and fluidic jets were deliberately chosen such that the fundamental oscillation produced by the fluidic device matched the subharmonic of the preferred mode for the primary jet. The excitation levels measured in the flow using the hot-film probe at $x/D_e = 0.6$ were 23, 14, 6, and 5% of the primary jet mean exit velocity U_0 for f, $2f$, $3f$, and $4f$, respectively.

The nozzle exit boundary layer of the primary nozzle, which is critical in determining the evolution of the jet,[10] was found to be fully turbulent (shape factor 1.56) with displacement and momentum thicknesses of $0.02827D_e$ and $0.01807D_e$, respectively. When the jet was excited in either the sinous or varicose mode, little or no change was seen in the state of the nozzle exit boundary layer.

Detailed cross-sectional maps of the velocity field at x/D_e of 3, normalized by U_0, are shown in Fig. 3 for the unforced rectangular jet (Fig. 3a) and the jet forced in the sinuous and varicose modes (Fig. 3b and 3c). For the forced jet cases the magnitude and relative size of the control jet flows, as well as their interaction with the primary jet flow, can be seen from the figure. It is observed that under excitation the jet spread and velocity decay occur more rapidly as compared to the unforced case. Note that under either condition of forcing the jet spreads more in the direction of its longer dimension.

The jet's centerline velocity and integrated mass-flux ratio are shown in Figs. 4a and 4b, respectively. Figure 4a indicates a more rapid decay of the jet's centerline velocity for the forced cases than for the unforced case, which is in agreement with Fig. 3. The mixing enhancement was quantified by calculating the integral mass flux from the cross-sectional flowfield data at various axial stations. The mass-flux ratio (Fig. 4b) illustrates that the fluidically excited jet entrains more air than the unforced jet. The increase in mass entrainment due to jet forcing appears to be about the same for either sinous or varicose excitation. The error bars shown were obtained using the uncertainty analysis methods described by Moffat.[11]

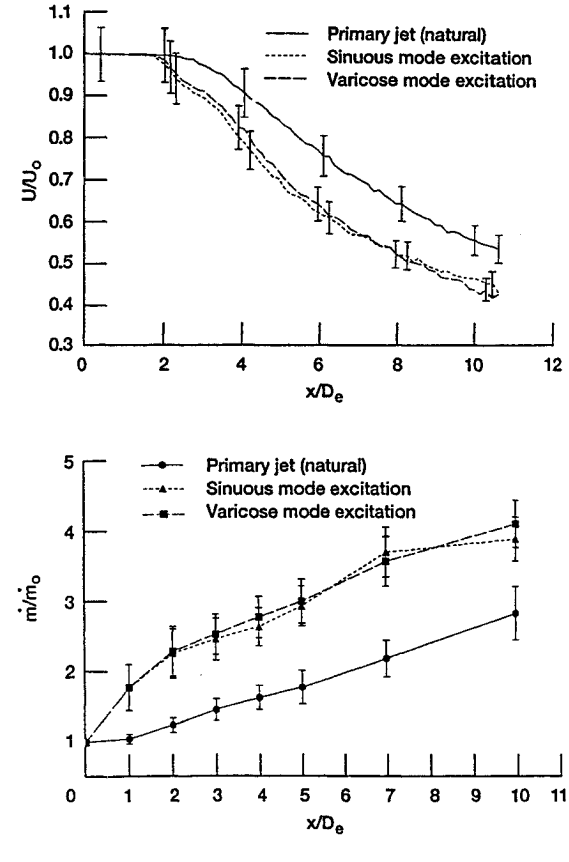

Fig. 4 Variation of jet centerline velocity and mass-flux ratio with axial distance: a) jet centerline velocity and b) mass-flux ratio.

Concluding Remarks

This research was motivated by a need for developing and applying practical excitation devices for the control of turbulent jets. The present investigation was designed to demonstrate that a jet flow could be forced by two miniature fluidic exciter jets. Two modes of excitation (sinuous and varicose) were applied at the subharmonic of the preferred frequency of the main jet flow. The primary jet had a turbulent nozzle exit condition, similar to the condition encountered in full-scale jet exhaust. The forcing technique presented in this work was successful in producing very large velocity perturbation levels in the main jet. Detailed maps of the main jet flowfield revealed that the jet's velocity decayed more rapidly for the forced cases than for the unforced. The normalized mass flux was higher for the forced cases than for the unforced, and both methods of jet excitation produced approximately the same increase in the mass-flux ratio. Shear flow excitation using flip-flop exciters appears to be promising for use in practical applications.

References

[1]Crow, S. C., and Champagne, F. H., "Orderly Structure in Jet Turbulence," *Journal of Fluid Mechanics*, Vol. 48, Aug. 1971, pp. 547–591.

[2]Raman, G., Zaman, K. B. M. Q., and Rice, E. J., "Initial Turbulence Effect on Jet Evolution with and without Tonal Excitation," *Physics of Fluids A*, Vol. 1, July 1989, pp. 1240–1248.

[3]Viets, H., "Flip-Flop Jet Nozzle," *AIAA Journal*, Vol. 13, No. 10, 1975, pp. 1375–1379.

[4]Rice, E. J., and Zaman, K. B. M. Q., "Control of Shear Flows by Artificial Excitation," AIAA Paper 87-2722, 1987.

[5]Raman, G., Hailye, M., and Rice, E. J., "Flip-Flop Jet Nozzle Extended to Supersonic Flows," *AIAA Journal*, Vol. 31, No. 6, 1993, pp. 1028–1035.

[6]Raman, G., Rice, E. J., and Cornelius, D., "Evaluation of Flip-Flop Jet Nozzles for Use as Practical Excitation Devices," *Journal of Fluids Engineering, Transactions of the ASME,* Vol. 116, 1994, pp. 508–515.
[7]Raman, G., and Rice, E. J., "Development of Phased Twin Flip-Flop Jets," *Journal of Vibration and Acoustics, Transactions of the ASME,* Vol. 116, 1994, pp. 263–268.
[8]Davis, M. R., "Variable Control of Jet Decay," *AIAA Journal*, Vol. 20, No. 5, 1982, pp. 606–609.
[9]Brown, W. H., and Ahuja, K. K., "Jet Mixing Enhancement by Hydrodynamic Excitation," AIAA Paper 90-4005, 1990.
[10]Lepicovsky, J., and Brown, W. H., "Effects of Nozzle Exit Boundary Layer Conditions on Excitability of Heated Jets," *AIAA Journal,* Vol. 27, 1989, pp. 712–718.
[11]Moffat, R. J., "Using Uncertainty Analysis in the Planning of an Experiment," *Journal of Fluids Engineering, Transactions of the ASME*, Vol. 114, 1985, pp. 362–366.

Turbulent Manipulation of Condensation at a Shock Tube's Contact Surface

Upul De Silva,* Aric Gardner,†
and
Joseph A. Johnson III‡
Florida Agricultural and Mechanical University, Tallahassee, Florida 32310

Introduction

An improved understanding of condensation phenomena in gaseous flow would have tremendous application to technological and scientific problems including droplet induced erosion in turbine blades, production of undesirable environmental conditions due to the condensation trails left by jet engines, and the inhibition of combustion in combustors. The usefulness of the shock tube for condensation studies was established by Wegener and Lundquist[1] followed by Glass and Patterson,[2] Barschdorff,[3] Sislian and Glass,[4] Kotake and Glass,[5] and Glass et al.[6] The development of the theory of nucleation rate and growth rate of the clusters is elaborated in the work of Lothe and Pound,[7,8] Dunning,[9] Wegener,[10] and Refs. 11–15. In recent experiments carried out by Britan et al.,[16] the effects of condensation on the parameters of the flow behind shock waves in water vapor were investigated in detail. Another recent experiment conducted by Schnerr and Bohning[17] investigated the effects of the heat addition by homogenous condensation on the compressible turbulent boundary layer. Nonetheless, in spite of all of this work, the relationship between the governing thermodynamic parameters and the simplest parameters in nucleation (such as onset and droplet growth rate) is not well understood at all.

It is particularly clear that no experimental treatment has determined either the role which turbulence plays in the observations, if any, or the implications for such a possible role in the development of a reliable physical model. Implicitly, all current theories for droplet sizes also assume no role for turbulence. We, therefore, examine in this paper the possibility of a relationship between condensation and turbulence using the reliable and predictable turbulent environment of a shock tube's contact surface as a test system for water vapor condensation. We do not concern ourselves, at this juncture, with the onset of condensation. Our main interest is to investigate experimentally the effect that turbulence has on an existing condensation front which is moving with the turbulent gaseous media.

Received Feb. 25, 1994; revision received Oct. 19, 1994; accepted for publication Oct. 19, 1994.

*Graduate Research Assistant, Department of Mechanical Engineering, College of Engineering. Student Member AIAA.
†Undergraduate Research Assistant, Department of Physics.
‡Distinguished Professor of Science and Engineering. Associate Fellow AIAA.

Experimental Facilities and Test Conditions

A pressure driven shock tube (Fig. 1) consisting of a driver section of 60 × 5.2 in., a driven section with a test section of 60 × 5.2 in., and an extension tube of 76 × 5.2 in. was used to carry out the experiment. Aluminized Mylar® sheets of various thicknesses were used as the material for the diaphragm which separates the driver section from the driven section. The compressed air is supplied to the driver section from a reservoir where the relative humidity of the air could be controlled by controlling the temperature in the driver gas. A heating tape is wrapped around (outside) the entire driver section, and a thermocouple probe is used in the driver section to measure the initial temperature.

The test section has three stations for optical diagnostics, two of which consist of four perpendicular glass ports; the other station has two inline glass ports. The test section is also equipped with several ports for pressure transducers. A 50-mW He-Ne laser is used for right-angle scattering through the optical station which is 2.5 ft downstream of the diaphragm. Two pressure transducers are mounted on either side of the optical station, 2 ft apart; pressure histories along with histories of the scattered signal at right angles are recorded on a four-channel 500-MHz Tektronix digital oscilloscope. All of the signals are stored on floppy disks. The optics for receiving the scattered signal from the droplets (Fig. 1b, no. 3) included a neutral density filter; the received signals are transmitted to the photomultiplier tubes using fiber optics and also stored on the oscilloscope just mentioned.

It has already been shown that in a pressure driven shock tube at a shock wave velocity of $M = 1.8$ the contact surface is fully turbulent.[18] A TSI three-dimensional laser doppler velocimeter (LDV) system is used to confirm the existence of turbulence in all three components of the local velocity at the contact surface; it consists of a 6-W Ar-ion laser, a color separator, a color link (photo multiplier tubes and amplifiers), a burst correlator (signal processor) and a 486 computer controller. For seeding the flow, 0.8-μm latex particles and incense smoke were used on both driver and driven sections. The overall data rate for the LDV during the approximately 500 μs of turbulent flow (all components) exceeded 30 kHz. Fourier analysis of the velocity fluctuations (all components) showed turbulent fluctuation spectra and turbulent autocorrelation profiles consistent with the results previously reported on density fluctuations in Ref. 18. The typical turbulent environment

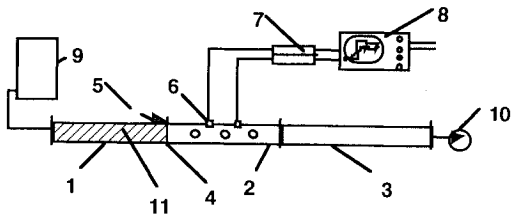

Fig. 1a Shock tube schematic: 1) driver section, 2) test section, 3) extension tube, 4) position of diaphragm, 5) plunger, 6) quartz pressure transducers, 7) signal amplifiers, 8) digitizing oscilloscope, 9) high-pressure tank, 10) vacuum pump, and 11) heating tape.

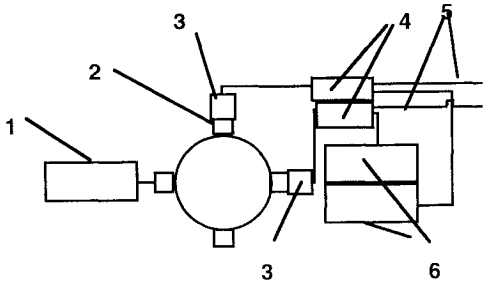

Fig. 1b Cross section of optical station showing right-angle scattering system (LDV setup not shown): 1) 50-mW He-Ne laser, 2) optical ports of the test section, 3) receiving optics, 4) phase modulated transmitter, 5) cables to oscilloscope, and 6) high-voltage power supplies.